Eur. Phys. J. A (2013) **49**: 61
DOI 10.1140/epja/i2013-13061-4

THE EUROPEAN PHYSICAL JOURNAL A

Special Article – Tools for Experiment and Theory

Correction for hole trapping in AGATA detectors using pulse shape analysis

for the AGATA Collaboration
B. Bruyneel[1,2,a], B. Birkenbach[2], J. Eberth[2], H. Hess[2], Gh. Pascovici[2], P. Reiter[2], A. Wiens[2], D. Bazzacco[3], E. Farnea[3], C. Michelagnoli[3], and F. Recchia[3]

[1] CEA Saclay, DSM/IRFU/SPhN, Gif-sur-Yvette Cedex, France
[2] Institut für Kernphysik, Universität zu Köln, Köln, Germany
[3] INFN, Sezione di Padova, Padova, Italy

Received: 14 December 2012 / Revised: 11 April 2013
Published online: 22 May 2013 – © Società Italiana di Fisica / Springer-Verlag 2013
Communicated by D. Pierroutsakou

Abstract. Data from the highly segmented High-Purity Germanium (HPGe) detectors of the AGATA spectrometer show that segments are more sensitive to neutron damage than the central core contact. Calculations on the collection efficiency of charge carriers inside the HPGe detector were performed in order to understand this phenomenon. The trapping sensitivity, an expression based on the collection efficiencies for electrons and holes, is put forward to quantify the effect of charge carrier trapping. The sensitivity is evaluated for each position in the detector volume with respect to the different electrodes and the collected charge carrier type. Using the position information obtained by pulse shape analysis from the position-sensitive AGATA detectors, it is possible to correct for the energy deficit employing detector specific sensitivity values. We report on the successful correction of the energy peaks from heavily neutron-damaged AGATA detectors for core and segment electrode signals. The original energy resolution can optimally be recovered up to a certain quantifiable limit of degradation due to statistical fluctuations caused by trapping effects.

1 Introduction

N-Type HPGe detectors have the reputation to be less sensitive to neutron damage than p-type detectors [1,2]. Besides the fact that large-volume coaxial detectors can be constructed with thinner outer contacts, this is a strong reason why typically n-type detectors are preferred over p-type for γ-ray spectroscopy applications which are potentially affected by the presence of neutrons. However, this customary reasoning recently has lost some of its value. The argument is only valid for the signal of the central core contact which is typically read out. For modern state-of-the-art spectrometers like AGATA [3–6] and GRETA [7, 8] the outer contact of the large-volume HPGe detectors is highly segmented. Net charge signals from these outer contacts are caused by electron and hole migration. These charge signals are simultaneously read out together with the core contact. The segmentation provides essential information for Pulse Shape Analysis (PSA) allowing to locate the individual interaction positions of gamma-rays inside the germanium volume with a precision of about 4 mm FWHM [9]. The three-dimensional position coordinates of the interaction points are the prerequisite for the following γ-ray tracking procedure. It is found that segments are more sensitive to neutron-induced traps than the core electrode.

This behaviour was observed during the first weeks of the experimental campaign with the AGATA demonstrator at Legnaro. The new HPGe crystals were exposed for the first time to the flux of fast neutrons from deep inelastic collisions, fission and fusion evaporation reactions. Fast neutrons are well known to produce specific lattice defects in germanium crystals which act as efficient hole traps. This leads to a reduction in the charge collection efficiency of the detectors evidenced by a low-energy tailing on the energy line shape. During the first three weeks of beam in Legnaro, the core decreased slightly in energy resolution from 2.3 keV to 2.4 keV. The segments resolution in contrast deteriorated on average from 2.0 keV to 3.0 keV. This indicates a large difference in sensitivity for hole trapping of the outer segments compared to the core electrode.

As the increased sensitivity of the segments to hole trapping was originally not taken into consideration, the above observation was surprising and triggered the work presented here. We will show in this paper how the sensitivity to trapping of both core and segments can be

[a] e-mail: bart.bruyneel@cea.fr

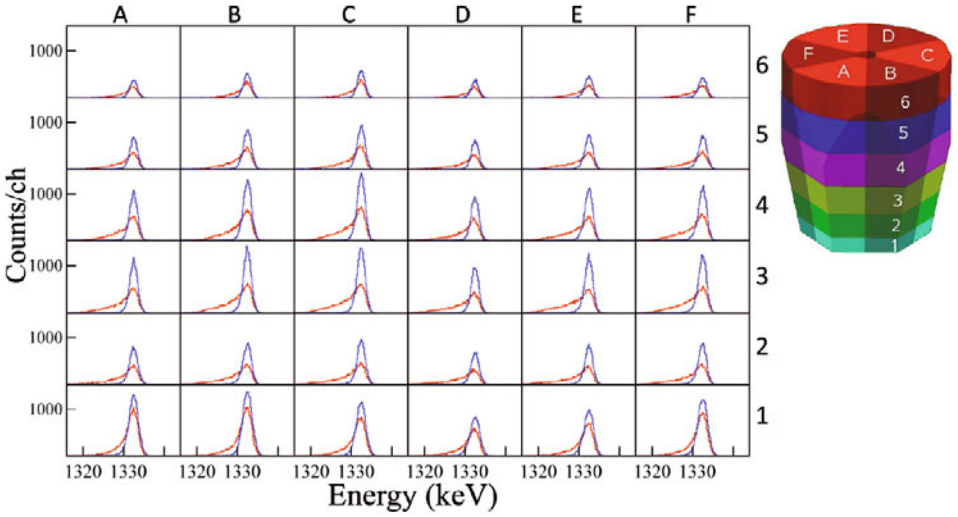

Fig. 1. Line shape of the segments of an AGATA detector at the end of the experimental campaign at Legnaro. Without correction for the neutron-induced hole trapping, pronounced left tails on all segments are observed (red). Using the correction procedure as described in this paper, a Gaussian line shape can be recovered (blue). The inset shows the geometry of an AGATA crystal and the labeling convention for the segments.

calculated. The peak height deficiency due to trapping can be determined as function of the interaction position of the gamma-rays within the crystal. Such calculations will be shown adequate to explain the difference in response between core and segment electrodes and allow for a correction of the effect.

The degradation near the end of the AGATA campaign at Legnaro is shown in fig. 1 for one AGATA detector (C002). This plot shows the segment line shapes for the 1333 keV ^{60}Co line. The pronounced left tail observed on all segments (in red) can be attributed to a neutron fluence estimated at $(7 \pm 1) \cdot 10^8$ neutrons/cm^2 (see sect. 6). The segmentation pattern and labeling convention of this detector is shown in the inset. More details on the detector geometry can be found in [6].

The crystals can recover from neutron damage by annealing. However, for practical reasons and in view of the rate at which neutron damage becomes visible, this treatment cannot be applied after every experiment. Correction methods were therefore developed in the past [10] aiming to minimize the unwanted effects due to trapping as much as possible, in-between consecutive annealing procedures. These methods have gained renewed interest [11,12] with the arrival of digital front-end electronics which opened access to the required position information. Fortunately, pulse shape analysis is not influenced by neutron trapping [12]: PSA is only sensitive to changes in the signal shape of the level of some percent, while the energy resolution is already sensitive below one part per thousand. Therefore energy resolution will be deteriorated far earlier than it will be noticed in the position resolution. Since the peak height deficiency will in first approximation only depend on the interaction position in the detector, the high position sensitivity of the AGATA array allows to make corrections for trapping effects using the pre-calculated trapping sensitivities.

As a preview to what is possible using such correction method, the line shapes after correction for trapping effects are also included in fig. 1 (in blue). The peak integral before and after correction is conserved to easily see the improvement in line shape. Variations in peak height further are reflecting the differences in peak detection efficiency of the various segments.

Although the correction for neutron-induced hole trapping was of primary interest, it should be noted that the developed models and methods described in the next sections are of general validity and are not restricted to specific trapping models or detector geometries. A short review of commonly used trapping models is therefore included in the next section.

2 Trapping and trapping rates

A good overview of the trapping mechanism is given in [13]. The most common model to describe trapping is probably the cascade model by Lax [14], although other models exist, see, *e.g.*, [15]. In the cascade model, the trapping proceeds in two steps. In the first step, a charge carrier emits a phonon near a trap center at which the charge gets loosely bound in one of the near-continuum states of the trapping center. The time after this will be decisive as the charge is in interaction with the phonon field at thermal energies. During this second step, the charge can either be released from the trap or it will collapse into the ground state of the trap. This second process is described by a sticking probability.

The trapping rate at a specific position along the collection path of the free local charge $q_{e,h}$ in the detector with trap density $N_{e,h}$ is given by

$$\frac{\mathrm{d}}{\mathrm{d}t} q_{e,h}(t) = -\langle \sigma v \rangle N_{e,h} q_{e,h}(t). \qquad (1)$$

The term $\langle\sigma(v)\cdot v\rangle$ consists of the microscopic trapping cross section $\sigma(v)$, which depends on the pre-collisional speed v of the electron(e)/hole(h). The expression is averaged over all populated states, a distribution which depends on the external field E. The trapping cross section itself is also field dependent (Poole-Frenkel effect [13]), which gives typically an average of the form

$$\langle\sigma v\rangle \ \propto E^x\langle v^y\rangle, \tag{2}$$

with x,y real numbers depending on the nature of the trapping centre.

In the specific case of fast neutron-induced trapping centers, Darken *et al.* [16] proposed a very appealing model. Fast neutrons above 1 MeV produce clusters of defects in the lattice which form the primary source of trapping. Since the net charge state Q of such cluster is negative, only holes are affected by these traps. As the Coulomb force of such highly charged traps can extend appreciably into the micrometer scale, a macroscopic model was proposed by Darken *et al.* for this particular trapping process, in contrast to the microscopic models discussed before. The cross section σ can then simply be calculated to be proportional to the radius at which the external field strength E is balanced by the Coulomb field of the trapping center. With ε the dielectric constant of germanium, this yields

$$\sigma = \frac{Q}{\varepsilon E}\,. \tag{3}$$

Given this is a pure macroscopic model, in which it is assumed that the charges at micrometer scale follow the field lines, we logically extend this thought by assuming that the trapping rate will be proportional to the hole drift velocity v_h. This is different from [1] which assumes that the rate will be proportional to $\langle v\rangle$. Our full assumption on the hole trapping rate specific to neutron-induced trapping centers therefore yields

$$\langle\sigma v\rangle = \alpha\frac{v_h}{E}\,, \tag{4}$$

with $\alpha = Q/\varepsilon$. A rough estimate on α can be calculated using the value cited in [16] of $Q \approx 100e$ for neutron-damage–induced traps in thermal equilibrium. This yields

$$\alpha \approx \ 2\cdot 10^{-9}\,\mathrm{kVcm}. \tag{5}$$

In this text, it is assumed that de-trapping effects can be neglected. We argue in the following way: in case de-trapping occurs at times longer than the shaping time of the acquisition, it will not be observed in the energy resolution. Contrarily, if it happens before the shaping time, it can be considered as if the trapping never happened. Consequently, assuming an effective trapping rate which depends on the shaping time, de-trapping effects can be neglected.

3 Collection efficiency

The method for trapping correction depends strongly on an accurate and position-dependent prediction of the charge induction in a particular electrode of the detector. The following derivations can be interpreted as a generalization of the calculations by Raudorf *et al.* [1], which addressed true coaxial detectors. The calculation here is not restricted to specific geometries nor to specific trapping centers.

The collection efficiency for a certain interaction position in the detector is defined as the ratio between the total amount of induced charge measured in a specific electrode and the amount of these charges initially created. According to eq. (1) the free charge carriers q created after radiation impact at $t = 0$ decrease exponentially along their path towards the collecting electrode

$$q_{e,h}(t) = q_{e,h}(0)\cdot\exp\left[-\int_0^t\langle\sigma v\rangle N_{e,h}\ \mathrm{d}t'\right]. \tag{6}$$

The density of trapping centers $N_{e,h}$ will change during experiments and it can be used as a parameter to model the observed trapping effect. This density will scale with the neutron dose applied to the detectors which can be monitored simply with the aid of neutron dosimeters [17] or by monitoring the specific Ge or Al de-excitation lines [18].

The collection efficiency for the i-th electrode, independently of its geometry, can be written as

$$\eta^i_{tot}(\boldsymbol{x}_0) = \eta^i_e(\boldsymbol{x}_0) + \eta^i_h(\boldsymbol{x}_0), \tag{7}$$

with

$$\begin{aligned}\eta^i_{e,h}(\boldsymbol{x}_0) &= \left|\int_0^{t_{col}}(\boldsymbol{\nabla}\phi_i(\boldsymbol{x}(t))\cdot\boldsymbol{v}_{e,h})\ \frac{q_{e,h}(t)}{q_{e,h}(0)}\mathrm{d}t\right| \\ &= \left|\int_0^{t_{col}}(\boldsymbol{\nabla}\phi_i(\boldsymbol{x}(t))\cdot\boldsymbol{v}_{e,h})\,e^{-\int_0^t\langle\sigma v\rangle N_{e,h}\mathrm{d}t'}\,\mathrm{d}t\right|.\end{aligned} \tag{8}$$

Equation (7) states that the total collection efficiency $\eta^i_{tot}(\boldsymbol{x}_0)$ for an interaction at position $\boldsymbol{x}_0$ is constituted out of the partial collection efficiencies for collecting electrons and holes. The partial efficiencies are expressed in eq. (8) using the Shockley-Ramo theorem [19,20] for a unit of charge deposited at $\boldsymbol{x}_0$ and with $\phi_i(\boldsymbol{x})$ the weighting potential for electrode i of interest. The right-hand side expresses the induced charge in electrode i as the integral of the current induced in this electrode by the movement of the free charge (with drift velocity $\boldsymbol{v}_{e,h}$) during the collection time t_{col}. Finally the absolute value in eq. (8) was taken to ensure the collection efficiency is a positive value, while otherwise the value would be depending on the sign of the charge.

4 Sensitivity to trapping

In the case of negligible trapping, the total collection efficiency in eq. (7) equals 1 for a hit electrode, 0 if not hit. Deviations from these values below the part per thousand level are important for high-resolution germanium detectors. The partial collection efficiencies in eq. (7) can take any value between 0 and 1. Their value is mainly position

dependent and reflects the properties of the weighting potential. Of interest are basically only the much smaller trapping-dependent deviations from the ideal partial collection efficiencies. These deviations can be isolated using a Taylor expansion of eq. (8) in the limit of a small trap density. This is a very practical move as we will show here that a Taylor expansion removes the need to recalculate the double integral eq. (8) on an event by event basis, which finally allows to make online corrections.

Although higher orders can also be calculated, a first order expansion will usually be sufficient. Limiting our expansion of eq. (7) to first order yields for hit electrodes

$$\eta^i_{tot}(\boldsymbol{x}_0) \cong 1 - \left[N_e s^i_e(\boldsymbol{x}_0) + N_h s^i_h(\boldsymbol{x}_0)\right], \tag{9}$$

$$s^i_{e,h}(\boldsymbol{x}_0) := \left|\frac{\mathrm{d}\eta^i_{e,h}}{\mathrm{d}N_{e,h}}|_{N_{e,h}=0}\right|. \tag{10}$$

This Taylor expansion separates out the *a priori* unknown trap density concentrations. The remaining factors $s^i_{e,h}(\boldsymbol{x}_0)$ are only dependent on the position in the detector. They are calculated in advance and mapped out over the whole detector volume. Equation (9) yields a practical method for online correction of trapping. We will further refer to the function $s^i_{e,h}(\boldsymbol{x}_0)$ as the sensitivity of electrode i to electron or hole trapping. As can be inferred from eq. (9) that sensitivities are necessarily positive quantities, the absolute value in the definition 10 can be used.

Defining $I_{e,h}(t)$ as the fraction of trapped particles at time t per unit trap density

$$I_{e,h}(t) := \int_0^t \langle\sigma v\rangle \mathrm{d}t', \tag{11}$$

we obtain the following expression for the sensitivity, using eq. (8) and definition (10):

$$s^i_{e,h}(\boldsymbol{x}_0) = \left|\int_0^{t_{col}} (\boldsymbol{\nabla}\phi_i \cdot \boldsymbol{v}_{e,h})\ I_{e,h}(t)\ \mathrm{d}t\right|, \tag{12}$$

$$= \left|I_{e,h}(t_{col})\phi_i(\boldsymbol{x}(t_{col})) - \int_0^{t_{col}} \phi_i(\boldsymbol{x}(t))\langle\sigma v\rangle \mathrm{d}t\right|. \tag{13}$$

The second eq. (13) can be proven by integration by parts. This expression is preferred over eq. (12) as the evaluation of the gradient is not required, which is simpler to compute and yields more accurate results.

Equation (13) also shows that the energy deficit consists of two parts: The first term in (13) corresponds to the fraction of charges that were not collected. The weighting potential at collection time takes on the value 1 or 0, depending on whether these particular charges were supposed to be collected at electrode i or not. The second term in (13) is the fraction originating from permanent induced charges from the trail of trapped charges distributed along the path in the detector.

The latter fraction will also induce signals in neighboring segments to the collecting electrodes. Due to the properties of the weighting potentials, the induced signal amplitudes in neighboring segments are typically one order of magnitude less than the signal loss observed in hit segments. Therefore, only in extremely neutron-damaged detectors [12], these second-order effects can be observed. We will therefore neglect the information in these smaller contributions for our correction method.

5 Sensitivity of an AGATA detector

To finally quantify the sensitivities, explicit values for the trapping cross sections are required. Since the factor α in eq. (4) is only approximately known, we will calculate the sensitivities for a reference value of $\alpha_0 = 1\,\mathrm{kVcm}$. If for a specific detector the value of α is known, the absolute sensitivities can be retrieved by scaling of the values with the ratio α/α_0. We will include the appropriate scaling factor in the units. With this convention, the sensitivity values take on the dimension $[\alpha/\alpha_0\,\mathrm{cm}^3]$ and the trapping center density takes on the dimension $[\alpha_0/\alpha\,\mathrm{cm}^{-3}]$.

Also the electron trapping sensitivities were calculated assuming a more general validity of eq. (4). This does not only allow a comparison between sensitivity of electron trapping to sensitivity of hole trapping. Electron trapping sensitivities which were calculated accordingly have shown recently the ability to correct for electron trapping phenomena observed in new AGATA detectors [21,22].

Under these assumptions, the sensitivities were evaluated using eq. (13). These equations were implemented in the AGATA detector simulation code (ADL) [23,24]. This code is used to generate the libraries of detector responses required by the PSA routines for the comparison and translation of pulse form data into position information. ADL is capable of calculating the hereto required weighting potentials, fields and drift velocities within the germanium volume. The code uses a 5th-order Runge-Kutta method to calculate the trajectories of electrons and holes created at specific interaction positions. These equations of motion were extended to the following set of 3 coupled differential equations from which the integrals (13) can be reconstructed,

$$\mathrm{d}\boldsymbol{x}_{e,h}/\mathrm{d}t = \boldsymbol{v}_{e,h}, \tag{14}$$

$$\mathrm{d}I_{e,h}/\mathrm{d}t = \langle\sigma v\rangle, \tag{15}$$

$$\mathrm{d}s^i_{e,h}/\mathrm{d}t = \phi_i(\boldsymbol{x}_{e,h}) \cdot \langle\sigma v\rangle. \tag{16}$$

The sensitivities for core and hit segment electrode are shown in fig. 2 under general assumption of eq. (4). Rather than showing 36 individual plots for each of the segments individually, the sensitivities for all segments were shown in one single graph, plotting only the sensitivity for the hit segment as function of the interaction position in the detector. This explains the wavy pattern following the segmentation lines in the detector.

Figure 2 shows that the segments are more sensitive to hole trapping than the core electrode as was observed experimentally. On the other hand,the core electrode is more

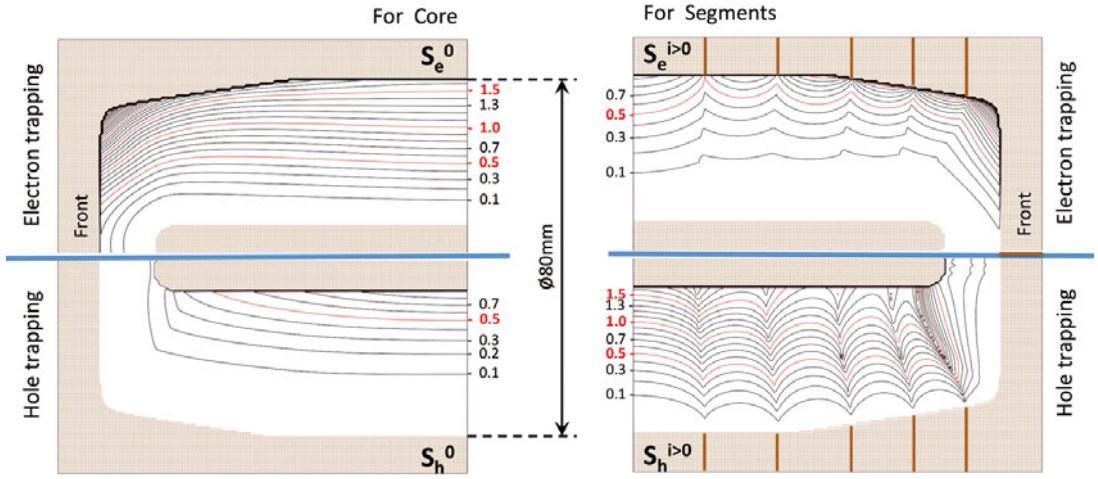

Fig. 2. Sensitivity plots for a cut throughout the center of the detector. Sensitivities for the core ($i = 0$) are shown on the left. Sensitivities for the segments ($i > 0$) are shown on the right. The two top pictures show sensitivities to electron trapping, while the two bottom pictures show sensitivities to hole trapping. The values were calculated in units of $[\alpha/\alpha_0\,\mathrm{cm}^3]$ for a reference value of $\alpha_0 = 1\,\mathrm{kVcm}$ as explained in the text.

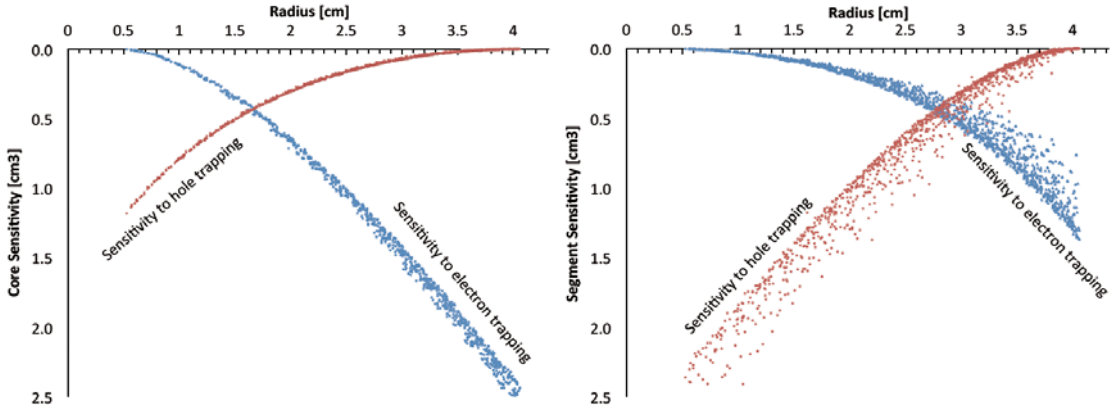

Fig. 3. Sensitivity to hole and electron trapping in the coaxial part of the detector (4 cm radius) as calculated from eq. (13). Left: sensitivities for the central core electrode. Right: Sensitivities for the hit segment electrode. All values were calculated in units of $[\alpha/\alpha_0\,\mathrm{cm}^3]$ for a reference value of $\alpha_0 = 1\,\mathrm{kVcm}$ as explained in the text.

sensitive to electron trapping than the segments. Since the trapping increases with the path length the charge carriers have to travel, also the sensitivity is increasing with the distance from the collecting electrode. Therefore the sensitivity to hole trapping is maximal near the core electrode and zero near the outer segment electrodes where the holes are immediately collected. The opposite is true for the electrons: the electron trapping sensitivity is maximal near the outer segment electrodes and zero near the central core electrode which collects the electrons.

Besides the dependence on the path length, these sensitivities are influenced by the shape of the weighting potential. This is obvious from fig. 3 which show the sensitivities as a function of radius in the coaxial part of the detector (radius = 4 cm) for a homogeneous distribution of points in that detector section. Other effects such as the anisotropic drift velocity have a negligible impact: The sensitivity of the core electrode is well parameterized by the radius only. The sensitivity of the segments *versus* radius shows a larger spread due to the angular dependence of the segment weighting potentials.

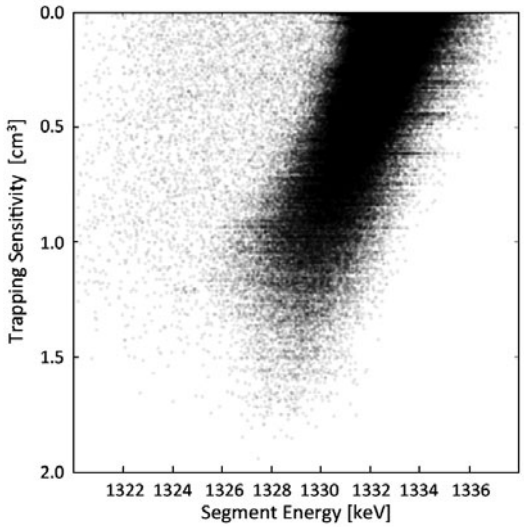

Fig. 4. Hole trapping sensitivity *vs.* segment energy correlation for 1333 keV gamma-rays from ^{60}Co. The sensitivity is evaluated from the interaction point provided by the PSA routines.

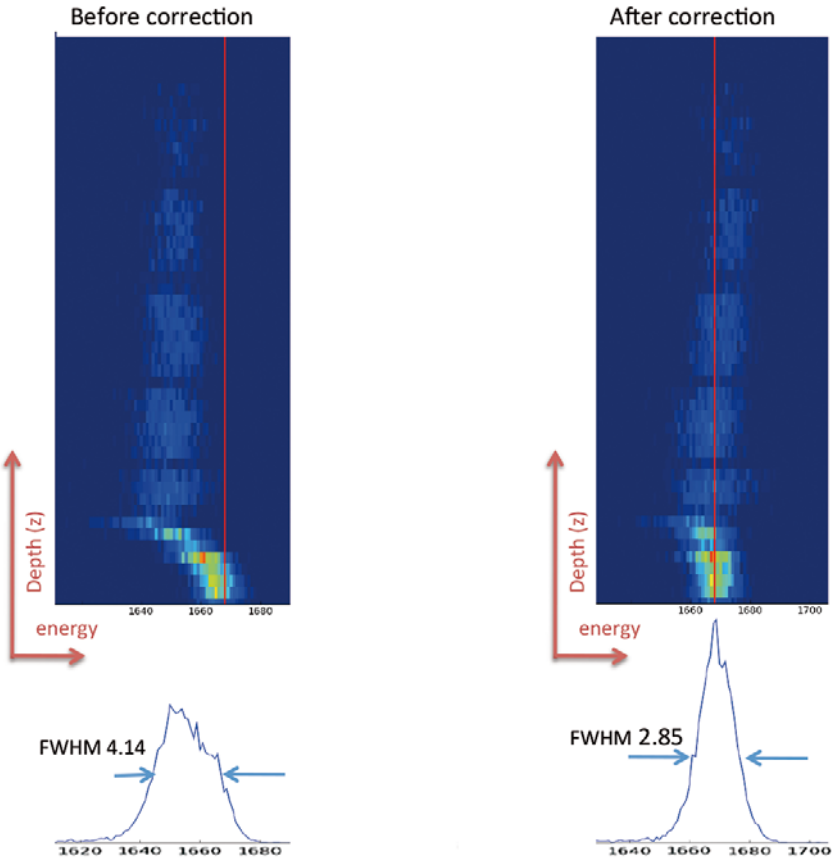

Fig. 5. Energy as function of depth in the detector for selected 1333 keV single events at 15 mm radius. Left, shifts in energy are visible due to the trapping process. The right plot is corrected for the hole trapping. The total depth of the crystal is 90 mm. At the bottom the projections for both plots are shown. (Energy axis not calibrated.)

6 Experimental results

We will validate the above theory using data from AGATA detector C002 taken with a ^{60}Co calibration source. The specifications of this detector can be found in [6]. At the point the data was recorded, the detector had suffered from a fair amount of neutrons, such that the major trapping process in the detector became fast neutron-induced hole trapping.

A straightforward evaluation and proof of the linear relationship between energy deficit due to hole trapping and the relevant sensitivity parameter s_h is obtained in fig. 4. The figure shows the correlation of the sensitivity values *versus* the single event segment energies, in a narrow interval around the 1333 keV ^{60}Co line. The sensitivity value is obtained exploiting the positions returned by the PSA. The correlation is strongly pronounced. Under the assumption of negligible electron trapping, a fit of this correlation yields the parameter N_h of eq. (9) as required for performing neutron damage corrections.

The dependence of the hole trapping rate on the position is further demonstrated in fig. 5 (left). For this density plot, single events with 1333 keV deposition were selected between 15 mm and 16 mm radius around the core. This radius was chosen as a compromise: the holes have to travel a relative long distance to the outer segments thus the effect of trapping is more pronounced, and yet the count rate at this radius is not too low. The energy registered by the segments for these selected events is plotted *versus* the depth in the detector. Without neutron damage, this plot would yield a straight vertical line at 1333 keV as indicated with the red line (not calibrated value at channel 1668). Due to neutron damage, these energies are shifted towards lower energies, proportional to the hole trapping sensitivity in fig. 2. The different behavior in the front of the detector comes from the fact that holes will be collected on the front face of the detector rather than traveling in radial direction.

The correction using eq. (9) assumes that N_h is a constant throughout the entire detector volume. This is argued in [1] to be a good approximation as the neutrons mean free path in germanium is about 6 cm. With this assumption, a two parameter fit for $N_{e,h}$ is performed using eq. (9) to optimize the resolution of the projection shown at the bottom of the graph. The same plot after correction for hole trapping is shown in fig. 5 (right). For the selected events, the energy distribution could be improved by this from 4.14 keV to 2.85 keV. A small remaining shift is still observed after correction indicating there might be a slight gradient in the distribution of the hole trap density. Obviously still a better result could be obtained assuming that $N_{e,h}$ varies as function of the hit segment.

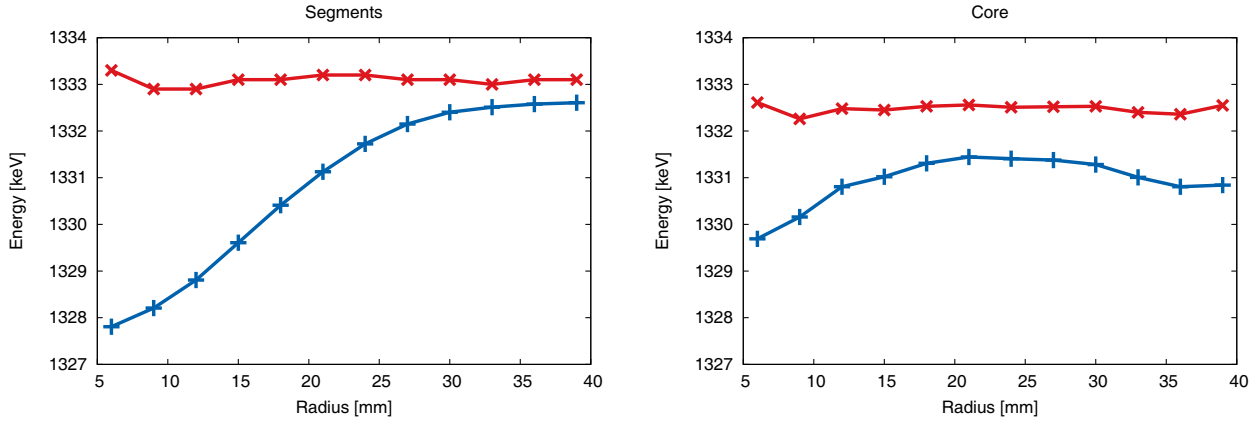

Fig. 6. Centroid of the full energy peak as a function of the interaction radius for selected 1333 keV single events in the coaxial part of the detector. Errors as determined by the fit were less than 50 eV. A pronounced peak shift for the segments can be seen on the left. The trapping effects are less severe for the core signal (right). The data without correction is plotted with "+" markers. The data after correction is plotted with "×" markers.

To show the radial dependence on trapping, all single events were selected for the 1333 keV line in the coaxial part of the detector ($z > 13$ mm). This is the region till where the core electrode extends. The events were sorted according to the interaction radius obtained from PSA in 12 equal bins ranging from 5 mm to 40 mm. At the same time, the sensitivity values corresponding to the interaction position of the events were equally sorted using the same binning. Spectra for each of the bins were constructed and the mean sensitivities per bin were calculated for further use in the analysis.

In fig. 6 the energy peak position is plotted for each bin as a function of the interaction radius. A very systematic behavior is observed both for core and segment electrodes. The uncorrected data show strong peak shifts near the core region. Remark the differences between the core energy shifts and the segment energy shifts. In the core data, a shift is also observed at larger radii. This is attributed to electron trapping, since hole trapping has no influence at this distance. Also in the segments this finite amount of electron trapping will need to be assumed.

The data in fig. 6 were fitted with eq. (9) and using the averaged sensitivities to obtain values for the unperturbed energy E_0 and the trapping densities N_h, N_e. The optimum values returned by the fits are listed in table 1. The data after correction for trapping effects using the tabulated fit parameters are also included in fig. 6. One observes that due to the correction an upward shift in the peak position will occur. This shift however will be small compared to the original tailing in the spectra. A simple recalibration procedure after correction should remediate this.

In all four fits, eq. (9) described the data sets well. The RMS value of the residuals in each fit was less than 0.13 keV. Within the obtained error bars, the same density values were deduced from all fits. Except maybe for a slight deviation of the hole trap density deduced from the core data. It is currently not clear why such a deviation could exist. Using the estimate of $\alpha \approx 2 \cdot 10^{-9}$ kVcm, we obtain an estimate for N_h of $N_h = 1 \cdot 10^6/\text{cm}^3$.

Table 1. Optimum fit parameters for the correction in fig. 6 using the trapping correction formula (9). Also fit parameters for the 1173 keV dataset are listed. Densities are in units of $\alpha_0/\alpha\,\text{cm}^{-3}$.

	Energy [keV]	E_0 [keV]	N_e $\times 10^{-4}$	N_h $\times 10^{-3}$
Seg	1333	1333.08 ± 0.17	5 ± 2	2.97 ± 0.12
Seg	1172	1173.71 ± 0.16	5 ± 2	2.98 ± 0.14
Core	1333	1332.49 ± 0.14	7.8 ± 0.9	3.8 ± 0.3
Core	1172	1173.04 ± 0.11	7.0 ± 0.7	3.7 ± 0.2

This method finally was successfully applied on-line during the first AGATA campaign with the AGATA demonstrator at Legnaro. The result of this novel correction method for the segments of detector C002 near the end of the beam campaign was already shown in the introductory part. The performance for all five position-sensitive triple-cluster detectors is demonstrated in fig. 7. Without correction for neutron damage, the core summed spectra had an energy resolution of 3.2 keV FWHM and 7.2 keV FWTM, which could be improved to 2.8 keV FWHM and 5.6 keV FWTM. The segments near the end of the campaign showed a dramatic left tailing. The uncorrected segment summed spectra showed a resolution of 5.5 keV FWHM and 15.5 keV FWTM. After correction for neutron damage, this could be strongly reduced to a final resolution of 2.9 keV FWHM and 6.8 keV FWTM. This result can be appreciated even better realizing that the summed spectra resolution for the undamaged detectors amounted to 2.5 keV FWHM and 4.8 keV FWTM.

The observed deterioration of the core energy resolution was used to finally estimate the accumulated neutron fluence during the Legnaro campaign. The energy

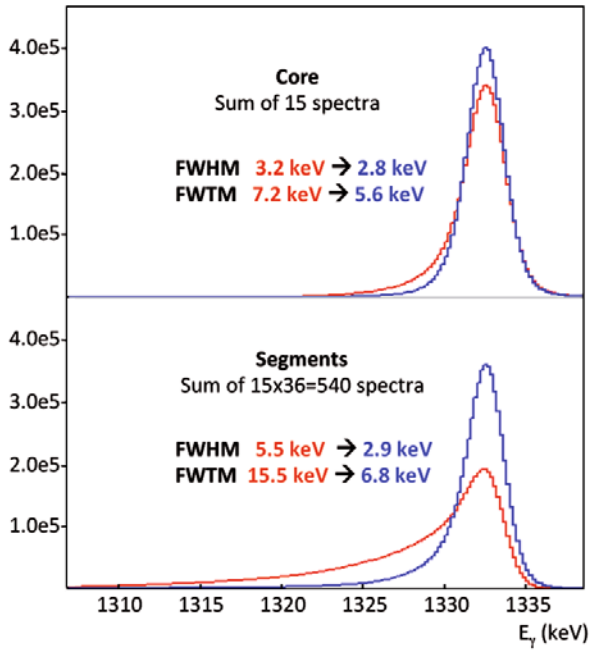

Fig. 7. The line shape of the summed core and segment energy spectra before (red) and after correction for trapping (blue). The spectra were taken at the end of the first AGATA beam campaign at Legnaro. The detectors were suffering heavily from neutron damage. Listed improvements need comparison with the summed resolution of undamaged detectors, which amounted to 2.5 keV FWHM and 4.8 keV FWTM.

degradation as function of neutron fluence was measured for a similar GRETA detector by Ross *et al.* [17]. From comparison to this data, we estimate a neutron fluence of $(7 \pm 1) \cdot 10^8$ neutrons/cm^2 responsible for the tailing in fig. 7.

7 Optimum energy resolution attainable

While eq. (9) allows to correct for the mean charge trapping, the trapping process remains statistical in nature. Such statistical fluctuations cannot be corrected for. This forms a limit upon which the energy resolution cannot be recovered. This extra broadening $\sigma_T(\boldsymbol{x}_0)$ adds up quadratically to the other contributions [1] which make out the final energy resolution of the detector,

$$\sigma(\boldsymbol{x}_0) = \sqrt{\sigma_N^2 + \sigma_F^2 + \sigma_T(\boldsymbol{x}_0)^2}\,, \qquad (17)$$

with σ_N the electronic noise and σ_F the statistical noise. The noise due to trapping $\sigma_T(\boldsymbol{x}_0)$ is position dependent and is expected to follow the relation

$$\sigma_T(\boldsymbol{x}_0) = \sqrt{\xi K E_0 [1 - \eta(\boldsymbol{x}_0)]}\,, \qquad (18)$$

with $\xi = 2.96\,\text{eV}$, and E_0 the total energy deposited in the detector. K is a constant, similar to the Fano factor which was estimated in [1] to be around $K = 340$. Studies on a new detector [21,22] however have shown that

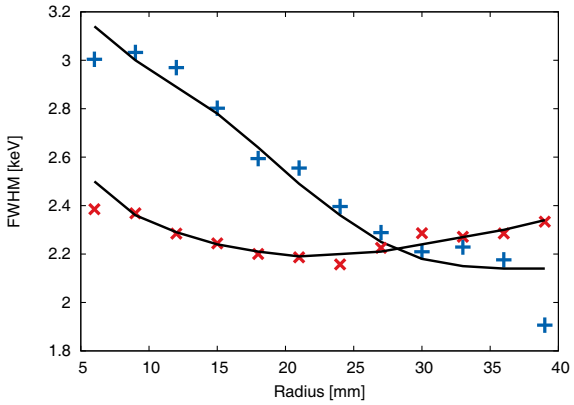

Fig. 8. Analysis of the FWHM resolution as function of radius for the 1333 keV Co line in the coaxial part of the detector. Errors on the data points were less than 50 eV. The segment data is plotted with "+" markers, while the core data is plotted with "×" markers. The solid lines corresponds to a fit using eq. (19).

Table 2. Optimum fit parameters used in fig. 8 for the fit formula (17). Also fit parameters for the 1173 keV dataset are listed.

	Energy [keV]	$2.35\,\sigma_0$ [keV]	K_h
seg	1333	2.03 ± 0.04	64 ± 5
seg	1172	1.97 ± 0.03	57 ± 4
core	1333	1.95 ± 0.01	51 ± 3
core	1172	1.92 ± 0.01	49 ± 3

the electron trapping follows this relation with a different K factor, namely $K = 59$. We therefore distinguish in eq. (18) between the different trapping mechanisms and propose the following generalization of eq. (18):

$$\sigma_T(\boldsymbol{x}_0) = \sqrt{\xi E_0 \left[K_e N_e s_e^i(\boldsymbol{x}_0) + K_h N_h s_h^i(\boldsymbol{x}_0)\right]}. \qquad (19)$$

To deduce the K_h value we look again to the single interaction events in the coaxial part of the detector. In fig. 8 the energy resolution for the 1333 keV ^{60}Co line is shown as function of radial position in the coaxial part of the detector. The solid lines correspond to the best fit obtained using eq. (17) and the averaged sensitivities as described before. The values on N_e and N_h were taken from table 1. The value K_e was fixed to 59 while K_h and $\sigma_0 = \sqrt{\sigma_N^2 + \sigma_F^2}$ were used as fitting parameters. The optimum fit parameters are listed in table 2.

In all four fits, eq. (17) appears adequate to describe the data. The RMS value of the residuals after fitting was less than 0.1 keV for the segment data and 0.02 keV for the core data. The larger RMS value of the segments is due to the last point which for unknown reason is deviating from the general trend. The fact that our measured K_h factors of about $K_h = 60$ is in large disagreement with the value $K_h = 340$ as obtained by Raudorf *et al.* [1] is surprising. We should point out that there are important differences

between the two analysis methods. While we could benefit from the high position sensitivity of our detector, yielding a rather direct measurement of the K_h value, the value derived by Raudorf *et al.* was obtained by a global fit to the line shape of a total-absorption peak.

On the other hand, the similarity of our K_h with the K_e factor, determined in a similar detector is also somewhat surprising, though it could have a physical meaning. If correlations in the trapping probability would exist between free charge carriers traveling close together, a larger K value would result. The fact that hole traps, which have a much larger cross section than the single site electron traps, still can be described with similar K values might be an indication that correlations in trapping still do not play a role even for the larger hole trapping cross sections.

8 Conclusion

The high position sensitivity of the AGATA detectors allows for correction of trapping effects. Such method was successfully demonstrated on the first AGATA detectors which suffered from neutron damage during the experimental campaign with the AGATA demonstrator at Legnaro. The segments show a higher sensitivity to hole trapping than the core. This experimental observation is in agreement with collection efficiency calculations. Therefore a definition for the trapping sensitivity is elaborated and proposed which is especially relevant for the new type of highly segmented, n-type HPGe detectors.

The sensitivities have shown to be very useful quantities. They provide a simple but accurate approximation to the collection efficiency in which the calculation intensive parameters can all be mapped prior to knowing the trap density distribution. This allows for an online correction of the trapping effects which will prolong the operation time of the detectors. The approximation can be calculated up to any precision although a first-order approximation has been found to yield satisfactory results for the level of irradiation of the studied detector.

Using data taken with an AGATA detector, it was shown that this method indeed allows to recover for the position dependence of the mean amplitude deficit in the detector. A simple two parameter optimization of the *a priori* unknown electron trap density and hole trap density is sufficient to describe the charge losses throughout the entire detector volume. The statistical variations in the charge loss however cannot be corrected for. This minimum loss in energy resolution is also position dependent and can be described as a function of the sensitivities. The experimental data compares very well with theory.

This research was supported by the German BMBF under Grants 06K-167 and 06KY205I. AGATA was supported by the European funding bodies and the EU Contract RII3-CT-2004-506065.

References

1. T.W. Raudorf, R.H. Pehl, Nucl. Instrum. Methods A **255**, 538 (1987).
2. Ortec manual, *The Best Choice of High Purity Germanium (HPGe) Detector*, `http://www.ortec-online.com/library/index.aspx`.
3. S. Akkoyun *et al.*, Nucl. Instrum. Methods A **668**, 26 (2012).
4. J. Simpson, J. Nyberg, W. Korten (Editors), *AGATA Technical Design Report* (2008), `https://www.agata.org/reports`.
5. E. Farnea *et al.*, Nucl. Instrum. Methods A **621**, 331 (2010).
6. A. Wiens *et al.*, Nucl. Instrum. Methods A **618**, 223 (2010).
7. I.-Y. Lee, J. Simpson, Nucl. Phys. News **20**, 23 (2010).
8. I.-Y. Lee, M.A. Deleplanque, K. Vetter, Rep. Prog. Phys. **66**, 1095 (2003).
9. F. Recchia *et al.*, Nucl. Instrum. Methods A **604**, 555 (2009).
10. M. Eschenauer *et al.*, Nucl. Instrum. Methods A **340**, 364 (1994).
11. W.C.G. Ho *et al.*, Nucl. Instrum. Methods A **412**, 507 (1998).
12. M. Descovich *et al.*, Nucl. Instrum. Methods A **545**, 199 (2005).
13. L. Reggiani, V. Mitin, Riv. Nuovo Cimento **12**, (1989).
14. M. Lax, Phys. Rev. **119**, 1502 (1960).
15. L.S. Darken, Phys. Rev. Lett. **69**, 2839 (1992).
16. L.S. Darken *et al.*, Nucl. Instrum. Methods **171**, 49 (1980).
17. T. Ross *et al.*, Nucl. Instrum. Methods A **606**, 533 (2009).
18. V. Borrel *et al.*, Nucl. Instrum. Methods A **430**, 348 (1999).
19. G.F. Knoll, *Radiation detection and Measurement*, 4th edition (Wiley & Sons).
20. W. Blum, W. Riegler, L. Rolandi, *Particle Detection with Drift Chambers* (Springer Verlag, 2008).
21. A. Wiens *et al.*, Eur. Phys. J. A **49**, 47 (2013).
22. A. Wiens, Doctoral thesis, University of Cologne (2011).
23. B. Bruyneel *et al.*, *AGATA Detector Library*, in preparation.
24. The ADL download page, `http://www.ikp.uni-koeln.de/research/agata/download.php`.